## NUMERICAL SOLUTION OF A TWO-DIMENSIONAL NONLOCAL WAVE EQUATION ON UNBOUNDED DOMAINS\*

QIANG DU†, HOUDE HAN‡, JIWEI ZHANG§, AND CHUNXIONG ZHENG‡

**Abstract.** We are concerned with the numerical solution of a nonlocal wave equation in an infinite two-dimensional space. The contribution of this paper is the derivation of an absorbing boundary condition which allows the wave field defined on the finite computational domain to retain the same feature as that defined on the original infinite domain. We resort to the idea of a first-kind integral equation method and develop a solution formulation in terms of a potential summation on a surrounding ghost region. This new formulation can be taken as an absorbing boundary condition of generalized Dirichlet-to-Dirichlet type. The accuracy and effectiveness of our approach are illustrated by some numerical examples.

**Key words.** nonlocal wave equation, nonlocal models, discrete absorbing boundary condition, artificial boundary method, Green's function, Dirichlet-to-Dirichlet mapping

AMS subject classifications. 82C21, 65R20, 65M60, 46N20, 45A05

**DOI.** 10.1137/16M1102896

1. Introduction. Recently, nonlocal models have received much attention in various research areas, such as the peridynamical theory of continuum mechanics, nonlocal wave propagation, and the modeling of nonlocal diffusion processes; see [6, 22, 36, 4, 1]. In this paper, we consider the Cauchy problem of the nonlocal wave equation in an infinite two-dimensional space:

(1.1) 
$$(\partial_t^2 + \mathcal{L}_{\delta}) q(\mathbf{x}, t) = f(\mathbf{x}, t), \ \mathbf{x} \in \mathbb{R}^2, \ 0 < t \le T,$$

(1.2) 
$$\partial_t^k q(\mathbf{x}, 0) = \psi_k(\mathbf{x}), \ \mathbf{x} \in \mathbb{R}^2, \ k \in \{0, 1\}.$$

In the above,  $q(\mathbf{x}, t)$  stands for the displacement field,  $\psi_k(\mathbf{x})$  (k = 0,1) are the initial values, and  $f(\mathbf{x}, t)$  is the body force. The linear operator  $\mathcal{L}_{\delta}$  is defined as

(1.3) 
$$\mathcal{L}_{\delta}q(\mathbf{x}) = \int_{\mathbb{R}^2} [q(\mathbf{x}) - q(\mathbf{y})]\gamma(\mathbf{x}, \mathbf{y})d\mathbf{y}$$

with some prescribed kernel function  $\gamma(\mathbf{x}, \mathbf{y})$ , which satisfies

(1.4) 
$$\gamma(\mathbf{x}, \mathbf{y}) \ge 0, \quad \gamma(\mathbf{x}, \mathbf{y}) = \gamma(\mathbf{y}, \mathbf{x}), \ \mathbf{x}, \mathbf{y} \in \mathbb{R}^2,$$

(1.5) 
$$\gamma(\mathbf{x}, \mathbf{y}) = 0, \ |\mathbf{x} - \mathbf{y}| > \delta.$$

Here  $\delta$  stands for the horizon of nonlocal effects.

http://www.siam.org/journals/sisc/40-3/M110289.html

Funding: The first author's work was supported in part by the U.S. NSF grants DMS-1719699 and CCF-1704833, AFOSR MURI Center for Material Failure Prediction Through Peridynamics, and OSD/ARO/MURI W911NF-15-1-0562 on Fractional PDEs for Conservation Laws and Beyond: Theory, Numerics and Applications. The third author's work was partially supported by NSFC under grants 11771035, 91430216, and U1530401. The fourth author's work was partially supported by NSFC under grant 11771248, 91630205,11371218.

<sup>\*</sup>Submitted to the journal's Methods and Algorithms for Scientific Computing section November 9, 2016; accepted for publication (in revised form) January 26, 2018; published electronically May 17, 2018.

<sup>&</sup>lt;sup>†</sup>Department of Applied Physics and Applied Mathematics, Columbia University, New York, NY 10027 (qd2125@columbia.edu).

<sup>&</sup>lt;sup>‡</sup>Department of Mathematical Sciences, Tsinghua University, Beijing 100084, China (hhan@math.tsinghua.edu.cn, czheng@math.tsinghua.edu.cn).

<sup>§</sup>Beijing Computational Science Research Center, Beijing 100193, China (jwzhang@csrc.ac.cn).

While most nonlocal works are carried out for bounded domain problems with volume constraints (see discussions in [5, 7, 10, 20, 24, 25, 36]), there exist situations in which simulations in an unbounded medium might be more reasonable, such as wave propagation in an exceedingly large sample. The unboundedness of the spatial domain presents a new computational challenge, since a naive spatial discretization generally leads to an infinite number of degrees of freedom for classical numerical methods such as finite element and finite difference methods.

The artificial boundary method (ABM) is one of the popular tools to deal with the unboundedness of domains; see the monograph [17] and review papers [11, 14, 28]. The main procedure of the ABM is to introduce artificial boundaries to restrict a bounded computational domain of interest, and then design suitable absorbing boundary conditions (ABCs) to eliminate waves which imping to the artificial boundary. Consequently, one can solve a reduced problem on bounded domains instead of the original problem on unbounded domains. As repeatedly shown in both theory and numerical experiments, the numerical accuracy strongly depends on the design of ABCs. Ideally, exact ABCs are those ensuring the solution of the reduced problem on bounded domains is the same as that of the original problem on unbounded domains. While the derivation of ABCs for linear local problems has been well studied, such as the exact ABCs [2, 3, 13, 16, 18, 23, 27, 21], the high-order local ABCs [11, 33, 30], the matching boundary condition [31], and so on, the computation of nonlocal problems on unbounded spatial domains has so far received little attention [34, 32, 35]. The main challenges lie in the selection of a suitable bounded computational domain and, above all, the construction of appropriate ABCs due to the nonlocal interactions.

The objective of this paper is to construct, in the spirit of ABMs, approximate ABCs for the nonlocal wave problem (1.1)–(1.2), and derive an effective numerical scheme. The main process to derive ABCs is as follows. We first discretize the problem (1.1)–(1.2) and deduce a semidiscrete nonlocal wave system in the infinite domain. After that, the Laplace transform is applied, leading to a discrete problem involving a complex variable  $z = s^2$  (s is introduced by the Laplace transform in section 4). For deriving ABCs of the semidiscrete system, we study the fundamental solution (discrete Green's function) of a reduced discrete exterior problem associated with the complex variable  $z = s^2$ . In analogy to the Poisson kernel for the Dirichlet boundary value problems of elliptic PDEs [19, 12], we then adopt the idea of the first-kind integral equation to express the solution of the discrete exterior problem by the potential summation. This equivalent formulation is in the form of a generalized Dirichlet-to-Dirichlet (DtD) type, and it can be considered as an exact ABC for the discrete system. When restricting this equivalent formulation to artificial boundary points, we finally reduce the original problem on the unbounded domain to a truncated nonlocal wave problem on a bounded domain.

The rest of this paper is as follows. We present a discrete nonlocal wave system in section 2, then design the corresponding ABCs by extending the idea of the Poisson kernel in section 3. In section 4, we use the Cauchy integral theorem to reformulate our ABCs into an integral formula, of which it is easy to take the inverse Laplace transform, to obtain a formulation in the physical space, and finally obtain a truncated time-dependent problem on a bounded domain. We use section 5 to introduce the basic setting of parameters and construct a numerical scheme, and present four numerical examples in section 6 to illustrate the efficiency of constructed ABCs and the convergence order of our numerical scheme. The conclusion is drawn in section 7.

2. Discrete nonlocal wave equation. We assume that the initial data  $\psi_k$  and the source function f are spatially compactly supported, and the kernel function  $\gamma$  becomes homogeneous at spatial locations suitably far away from the origin. With these assumptions, we know that there exists a positive number W and a function  $\gamma_0$  such that

(2.1) 
$$f(\mathbf{x},t) = 0, \ \psi_k(\mathbf{x}) = 0, \ k \in \{0,1\}, \ |\mathbf{x}| > W,$$
$$\gamma(\mathbf{x},\mathbf{y}) = \gamma_0(\mathbf{x} - \mathbf{y}), \ |\mathbf{x}| > W, \ |\mathbf{y}| > W - \delta.$$

We use  $|\cdot|$  to denote the maximum norm of a vectorial object here and hereafter. Due to the symmetry condition of  $\gamma$  in (1.4), it is easy to verify the following,

$$(\mathcal{L}_{\delta}q, p) = \frac{1}{2} \int_{\mathbb{D}^2} \int_{\mathbb{D}^2} [q(\mathbf{x}) - q(\mathbf{y})][p(\mathbf{x}) - p(\mathbf{y})] \gamma(\mathbf{x}, \mathbf{y}) d\mathbf{y} d\mathbf{x}.$$

The above formula implies that the nonlocal operator  $\mathcal{L}_{\delta}$  is symmetric and nonnegative. Using the same notation  $\mathcal{L}_{\delta}$  to denote its self-adjoint extension in  $L^{2}(\mathbb{R}^{2})$ , we know that the definition domain  $\mathcal{D}(\mathcal{L}_{\delta})$  of  $\mathcal{L}_{\delta}$  is given by

$$\mathcal{D}(\mathcal{L}_{\delta}) = \left\{ q \in L^{2}\left(\mathbb{R}^{2}\right) : \frac{1}{4} \int_{\mathbb{R}^{2}} \int_{\mathbb{R}^{2}} [q(\mathbf{x}) - q(\mathbf{y})]^{2} \gamma(\mathbf{x}, \mathbf{y}) d\mathbf{y} d\mathbf{x} < \infty \right\}.$$

Since  $\mathcal{L}_{\delta}$  is nonnegative definite, the spectrum  $\sigma(\mathcal{L}_{\delta})$  lies in the right real axis.

For the numerical solution of the problem (1.1)–(1.2), we first discretize the spatial variable to get an approximate semidiscrete system. There are many ways to derive spatial discretization for the nonlocal operator  $\mathcal{L}_{\delta}$ . To do benchmark studies on the numerical methods and to compare them with the local wave equations, it is interesting to consider the asymptotic compatibility (AC) property for the discrete nonlocal operator  $\mathcal{L}_{\delta,h}$ , since the nonlocal models can be taken as generalizations of the classical local models. It is desirable to have the quadrature discretization of  $\mathcal{L}_{\delta}$ maintaining this relationship. This implies that as the horizon parameter  $\delta$  tends to zero under some scaling conditions, the limit of the discrete nonlocal operator  $\mathcal{L}_{\delta,h}$ should be an approximation of the limiting continuous local operator. This issue has been intensively investigated in [24, 25, 26, 8]. For example, a quadrature-based finite difference scheme has been proposed in [8] and adopted in [26] to discretize the nonlocal term  $\mathcal{L}_{\delta}$  in the case that  $\gamma(\mathbf{x}, \mathbf{y}) = \gamma_0(\mathbf{x} - \mathbf{y})$  which is an extension of the onedimensional version given earlier in [24]. Let us denote by  $\mathcal{T}_h$  a uniform rectangular grid over the whole domain that is uniform in all directions with the same mesh size h and by  $\Phi_{\mathbf{n}}(\mathbf{x})$  the standard continuous piecewise bilinear basis function at point  $\mathbf{x_n} = \mathbf{n}h$ . At the node  $\mathbf{x_n}$  for  $\mathbf{n} \in \mathbb{Z}^2$ , the operator  $\mathcal{L}_{\delta}$  can be approximated by

(2.2) 
$$\mathcal{L}_{\delta,h}q(\mathbf{x_n}) = \int_{\mathbb{R}^2} \mathcal{I}_h\left(\frac{q(\mathbf{x_n}) - q(\mathbf{y})}{w(\mathbf{x_n} - \mathbf{y})}\right) w(\mathbf{x_n} - \mathbf{y}) \gamma_0(\mathbf{x_n} - \mathbf{y}) d\mathbf{y},$$

where  $\mathcal{I}_h$  represents the piecewise bilinear interpolation operator associated with the grid  $\mathcal{T}_h$ , and  $w(\mathbf{z})$  represents a weight function introduced in [26, 8] by

$$w(\mathbf{z}) = \frac{|\mathbf{z}|^2}{|z_1| + |z_2|}.$$

The introduction of the term  $w(\mathbf{z})$  in (2.2) is an important ingredient for extending the scheme constructed in [24] to the multidimensional case, thus assuring the so-called

AC property [25]. More detailed discussions can be found in [26, 8]. After a simple calculation, we can rewrite (2.2) as

(2.3) 
$$\mathcal{L}_{\delta,h}q(\mathbf{x_n}) = \sum_{\mathbf{m} \neq \mathbf{n}} \frac{q(\mathbf{x_n}) - q(\mathbf{x_m})}{w(\mathbf{x_n} - \mathbf{x_m})} \int_{\mathbb{R}^2} \Phi_{\mathbf{m}}(\mathbf{y}) w(\mathbf{x_n} - \mathbf{y}) \gamma_0(\mathbf{x_n} - \mathbf{y}) d\mathbf{y},$$

where the  $\{\Phi_{\mathbf{m}}(\mathbf{y})\}\$ , as in the above, are the hat basis corresponding to the piecewise bilinear interpolation operator. Applying the quadrature scheme (2.3) to the integral involved in  $\mathcal{L}_{\delta}$ , we have a discrete nonlocal operator  $\mathcal{L}_{\delta,h}$  given by

(2.4) 
$$\mathcal{L}_{\delta,h}q(\mathbf{x_n}) = \sum_{\mathbf{m} \in \mathbb{Z}^2} a_{\mathbf{n},\mathbf{m}}q(\mathbf{x_m}),$$

where

$$a_{\mathbf{n},\mathbf{m}} = \begin{cases} -\frac{1}{w(\mathbf{x_n} - \mathbf{x_m})} \int_{\mathbb{R}^2} \Phi_{\mathbf{m}}(\mathbf{y}) w(\mathbf{x_n} - \mathbf{y}) \gamma_0(\mathbf{x_n} - \mathbf{y}) d\mathbf{y}, & \mathbf{m} \neq \mathbf{n}, \\ \sum_{\mathbf{k} \neq \mathbf{n}} \frac{1}{w(\mathbf{x_n} - \mathbf{x_k})} \int_{\mathbb{R}^2} \Phi_{\mathbf{k}}(\mathbf{y}) w(\mathbf{x_n} - \mathbf{y}) \gamma_0(\mathbf{x_n} - \mathbf{y}) d\mathbf{y}, & \mathbf{m} = \mathbf{n}. \end{cases}$$

Replacing the continuous nonlocal operator  $\mathcal{L}_{\delta}$  in (1.1) with the above discrete counterpart (2.4), we derive the following approximate semidiscrete nonlocal wave system

(2.5) 
$$\partial_t^2 q_{\mathbf{n}} + \sum_{\mathbf{m} \in \mathbb{Z}^2} a_{\mathbf{n}, \mathbf{m}} q_{\mathbf{m}} = f(x_{\mathbf{n}}, t), \ \mathbf{n} \in \mathbb{Z}^2, \ 0 < t \le T,$$
(2.6) 
$$\partial_t^k q_{\mathbf{n}}(0) = \psi_k(\mathbf{x}_{\mathbf{n}}), \ \mathbf{n} \in \mathbb{Z}^2, \ k \in \{0, 1\}.$$

(2.6) 
$$\partial_t^k q_{\mathbf{n}}(0) = \psi_k(\mathbf{x_n}), \ \mathbf{n} \in \mathbb{Z}^2, \ k \in \{0, 1\}$$

In the above,  $q_{\mathbf{n}}(t)$  stands for the numerical approximation of  $q(\mathbf{x}_{\mathbf{n}}, t)$ .

In the current work, we mainly consider the case when the kernel  $\gamma$  is smooth and the horizon  $\delta$  is of order one. It is possible to further simplify the scheme (2.2) in the numerical implementation while maintaining the same accuracy. We leave this discussion to the section of numerical experiments.

By the finite horizon assumption (1.5), we have

$$a_{n,m} = 0, |n - m| > L,$$

for some constant L on the order of  $\lceil \delta/h \rceil$ . Also, by the symmetry property and the homogeneity assumption (2.1), putting  $M = \lceil W/h \rceil$ , we have

(2.7) 
$$f(x_{\mathbf{n}}, t) = 0, \ \psi_k(\mathbf{x_n}) = 0, \ |\mathbf{n}| > M, \ k \in \{0, 1\},$$
$$c_{\mathbf{m}} = a_{\mathbf{n}, \mathbf{n} + \mathbf{m}}, \ |\mathbf{n}| > M, \ |\mathbf{m}| \le L,$$

where  $c_{\mathbf{m}}$  is a grid function determined by  $a_{\mathbf{n},\mathbf{m}}$ .

Now the problem (2.5)-(2.6) can be decomposed into two subproblems which are coupled together. The first subproblem is defined on the index set with  $|\mathbf{n}| \leq M$ :

(2.8) 
$$\partial_t^2 q_{\mathbf{n}} + \sum_{|\mathbf{m} - \mathbf{n}| \le L} a_{\mathbf{n}, \mathbf{m}} q_{\mathbf{m}} = f(x_{\mathbf{n}}, t), \ |\mathbf{n}| \le M, \ 0 < t \le T,$$

(2.9) 
$$\partial_t^k q_{\mathbf{n}}(0) = \psi_k(\mathbf{x_n}), \ |\mathbf{n}| \le M, \ k \in \{0, 1\}.$$

The second subproblem is defined on the index set with  $|\mathbf{n}| > M$ :

(2.10) 
$$\partial_t^2 q_{\mathbf{n}} + \sum_{|\mathbf{m}| \le L} c_{\mathbf{m}} q_{\mathbf{n} - \mathbf{m}} = 0, |\mathbf{n}| > M, \ 0 < t \le T,$$

(2.11) 
$$\partial_t^k q_{\mathbf{n}}(0) = 0, \ |\mathbf{n}| > M, \ k \in \{0, 1\}.$$

Both of these subproblems are incomplete by themselves, since for the first subproblem (2.8)-(2.9), the quantities  $q_{\mathbf{n}}$  with  $|\mathbf{n}| > M$  involved in (2.8) are not prescribed, and for the second subproblem (2.10)–(2.11), the quantities  $q_{\mathbf{n}}$  with  $|\mathbf{n}| \leq M$  involved in (2.10) are not prescribed. However, if we can manage to express  $\{q_n\}_{|n|>M}$  with  $\{q_{\mathbf{n}}\}_{|\mathbf{n}|\leq M}$  through the second subproblem, by taking their relation as a boundary condition for the first subproblem, the first subproblem becomes closed, and it can then be integrated out with an ODE solver.

3. Reduced exterior problems. To derive an expression of  $\{q_n\}_{|n|>M}$  using the information of  $\{q_{\mathbf{n}}\}_{|\mathbf{n}| < M}$  through the second subproblem (2.10), we perform the Laplace transform and solve a sequence of reduced exterior problems to determine some DtD mappings. To achieve this, we resort to the idea of a first-kind integral equation and express the solution as a potential summation. To determine the potential density, we need to solve a linear system which involves all grid points located in the artificial boundary layer.

The reduced problem associated with the subproblem (2.10)–(2.11) is

(3.1) 
$$zu_{\mathbf{n}} + \sum_{|\mathbf{m}| \le L} c_{\mathbf{m}} u_{\mathbf{n} - \mathbf{m}} = 0, \ |\mathbf{n}| > M,$$
(3.2) 
$$\lim_{|\mathbf{n}| \to \infty} u_{\mathbf{n}} = 0,$$

$$\lim_{|\mathbf{n}| \to \infty} u_{\mathbf{n}} = 0,$$

where z is a complex parameter. Let us introduce the sequence space

$$\mathfrak{l}_{\mathbb{Z}^2} = \left\{ \vec{u} = \{u_{\mathbf{n}}\}_{\mathbf{n} \in \mathbb{Z}^2} : u_{\mathbf{n}} \in \mathbb{C}, \|u\|^2 = \sum_{\mathbf{n} \in \mathbb{Z}^2} |u_{\mathbf{n}}|^2 < \infty \right\},$$

and the linear subspace

$$\mathfrak{l}_{\mathbb{Z}^2}^c = \left\{ \vec{u} = \{u_{\mathbf{n}}\}_{\mathbf{n} \in \mathbb{Z}^2} \in \mathfrak{l}_{\mathbb{Z}^2} : u_{\mathbf{n}} = 0, \ |\mathbf{n}| \ge N \text{ for some } N > 0 \right\}.$$

The sequence space  $\mathbb{I}_{\mathbb{Z}^2}$  is a separable Hilbert space with the inner product

$$(\vec{u}, \vec{v}) = \sum_{\mathbf{n} \in \mathbb{Z}^2} u_{\mathbf{n}} \bar{v}_{\mathbf{n}}, \ \vec{u} = \{u_{\mathbf{n}}\}_{\mathbf{n} \in \mathbb{Z}^2}, \ \vec{v} = \{v_{\mathbf{n}}\}_{\mathbf{n} \in \mathbb{Z}^2},$$

where  $\bar{v}_{\mathbf{n}}$  represents the complex conjugate of  $v_{\mathbf{n}}$ . Let us define the linear operator  $\mathcal{T}$ on  $\mathfrak{l}_{\mathbb{Z}^2}^c$  as

(3.3) 
$$\mathcal{T}\vec{u} = \left\{ \sum_{|\mathbf{m}| \le L} c_{\mathbf{m}} u_{\mathbf{n} - \mathbf{m}} \right\}_{\mathbf{n} \in \mathbb{Z}^2}, \ \vec{u} = \{u_{\mathbf{n}}\}_{\mathbf{n} \in \mathbb{Z}^2}.$$

Notice that the operator  $\mathcal{T}$  is symmetric, nonnegative, and densely defined in  $\mathfrak{l}_{\mathbb{Z}^2}$ . By using the same notation  $\mathcal{T}$  to denote its self-adjoint extension, we know that the spectrum  $\sigma(\mathcal{T})$  lies in the right-half real axis.

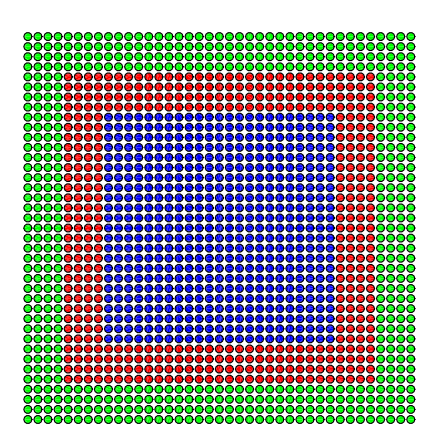


Fig. 1. Domain decomposition. The initial data functions and the source function are supported in the computational domain (M=15) which includes the blue zone and the red zone (L=4). The red zone represents the artificial boundary layers denoted by  $\mathcal{I}_b$ . The green zone expresses the set of ghost points denoted by  $\mathcal{I}_g$ . The nonlocal wave equation becomes homogeneous in the green zone. The ABCs are constructed on the green zone.

For all  $z \notin \sigma(-\mathcal{T})$  and prescribed  $u_{\mathbf{n}}$  for all boundary indices  $\mathbf{n} \in \mathcal{I}_b$  with

$$\mathcal{I}_b = \left\{ \mathbf{n} \in \mathbb{Z}^2 : M - L < |\mathbf{n}| \le M \right\},\,$$

the exterior problem (3.1)–(3.2) admits a unique solution which depends continuously on the data. In particular, there exists a sequence of operators

$$\mathcal{K}_{\mathbf{n},\mathbf{m}} = \mathcal{K}_{\mathbf{n},\mathbf{m}}(z), \ \mathbf{n} \in \mathcal{I}_g, \ \mathbf{m} \in \mathcal{I}_b$$

with (one can see Figure 1 for the basic settings)

$$\mathcal{I}_g = \left\{ \mathbf{n} \in \mathbb{Z}^2 : M < |\mathbf{n}| \le M + L \right\},\,$$

such that

(3.4) 
$$u_{\mathbf{n}} = \sum_{\mathbf{m} \in \mathcal{I}_b} \mathcal{K}_{\mathbf{n}, \mathbf{m}} u_{\mathbf{m}}, \ \mathbf{n} \in \mathcal{I}_g.$$

The sequence of operators  $\mathcal{K}_{\mathbf{n},\mathbf{m}}$  plays the role of DtD mappings for the reduced problem (3.1)–(3.2). It is generally hard to express  $\mathcal{K}_{\mathbf{n},\mathbf{m}}$  in a closed form. In the rest of this section, we will propose a numerical method to evaluate  $\mathcal{K}_{\mathbf{n},\mathbf{m}}$ . The main procedure is that we first study the fundamental solution (discrete Green's function) of a reduced discrete exterior problem associated with the complex variable z. Similarly to the poisson kernel for the Dirichlet boundary value problems of elliptic PDEs [19, 12], we then adopt the idea of the first-kind integral equation to express the solution of the discrete exterior problem by the potential summation.

**3.1. The fundamental solution.** The fundamental solution  $G_{\mathbf{n}} = G_{\mathbf{n}}(z)$  with  $z \notin \sigma(-\mathcal{T})$  for the governing equation of (3.1) solves the following problem:

(3.5) 
$$zG_{\mathbf{n}} + \sum_{|\mathbf{m}| \le L} c_{\mathbf{m}} G_{\mathbf{n} - \mathbf{m}} = \delta_{\mathbf{n}, \mathbf{0}}, \ \mathbf{n} \in \mathbb{Z}^2,$$

$$(3.6) G_{\mathbf{n}} \to 0, \quad |\mathbf{n}| \to \infty,$$

where  $\delta_{\mathbf{n},\mathbf{0}}$  stands for the Kronecker symbol. The fundamental solution  $G_{\mathbf{n}}$  plays a key role in the construction of ABCs in section 3.2. Performing the two-dimensional discrete Fourier transform onto (3.5), i.e.,

$$(\mathcal{F}G)_{\mathbf{k}} = \sum_{\mathbf{n} \in \mathbb{Z}^2} G_{\mathbf{n}} e^{-i\mathbf{n} \cdot \mathbf{k}}, \ \mathbf{k} \in \mathbb{R}^2,$$

we derive

$$(\mathcal{F}G)_{\mathbf{k}} = \left(z + \sum_{|\mathbf{m}| < L} e^{-i\mathbf{m} \cdot \mathbf{k}} c_{\mathbf{m}}\right)^{-1}.$$

The inverse transform on the periodic function  $\mathcal{F}G$  leads to

(3.7) 
$$G_{\mathbf{n}} = \frac{1}{4\pi^2} \int_{[0,2\pi]^2} \left( z + \sum_{|\mathbf{m}| \le L} e^{-i\mathbf{m} \cdot \mathbf{k}} c_{\mathbf{m}} \right)^{-1} e^{i\mathbf{n} \cdot \mathbf{k}} d\mathbf{k}, \ \mathbf{n} \in \mathbb{Z}^2.$$

There is an obvious need to develop some effective numerical technique to evaluate  $G_{\mathbf{n}}$ . Notice that the condition  $z \notin \sigma(-\mathcal{T})$  ensures a unique solution to the problem (3.5)-(3.6) which decays fast when  $|\mathbf{n}| \to \infty$ . Therefore, it is a natural choice to periodize the problem (3.5)-(3.6) by truncating the index set into a large enough rectangular domain. Equivalently, we approximate the fundamental solution  $G_{\mathbf{n}}$  by replacing the continuous inverse Fourier transform with its discrete counterpart. We should remark that the discrete inverse Fourier transform can be performed efficiently by the classical FFT algorithm.

**3.2. DtD mappings.** Resorting to the idea of a first-kind integral equation, we express the solution of problem (3.1)–(3.2) as a potential summation. Precisely, we determine the potentials  $f_{\mathbf{n}}$  for all  $\mathbf{n} \in \mathcal{I}_b$ , such that the following solution expression is valid:

(3.8) 
$$u_{\mathbf{n}} = \sum_{\mathbf{m} \in \mathcal{I}_b} G_{\mathbf{n} - \mathbf{m}} f_{\mathbf{m}}, \ |\mathbf{n}| > M - L.$$

Confined to the artificial boundary layer, we have

(3.9) 
$$u_{\mathbf{n}} = \sum_{\mathbf{m} \in \mathcal{I}_b} G_{\mathbf{n} - \mathbf{m}} f_{\mathbf{m}}, \ \mathbf{n} \in \mathcal{I}_b.$$

The above equation is a discrete analogue of the first-kind integral equation for the exterior Dirichlet boundary value problem. Let  $G^{-1} = (G_{\mathbf{n},\mathbf{m}}^{-1})$  be the inverse matrix of the matrix  $(G_{\mathbf{n}-\mathbf{m}})$  with  $\mathbf{n}, \mathbf{m} \in \mathcal{I}_b$  (the invertibility remains a theoretical issue). Then we have

$$f_{\mathbf{m}} = \sum_{\mathbf{k} \in \mathcal{I}_b} G_{\mathbf{m}, \mathbf{k}}^{-1} u_{\mathbf{k}}, \ \mathbf{k} \in \mathcal{I}_b.$$

Substituting the above into (3.8) yields

$$u_{\mathbf{n}} = \sum_{\mathbf{m} \in \mathcal{I}_b} \sum_{\mathbf{k} \in \mathcal{I}_b} G_{\mathbf{n} - \mathbf{m}} G_{\mathbf{m}, \mathbf{k}}^{-1} u_{\mathbf{k}}, \ |\mathbf{n}| > M.$$

In particular, this implies that

(3.10) 
$$\mathcal{K}_{\mathbf{n},\mathbf{m}} = \sum_{\mathbf{k} \in \mathcal{I}_b} G_{\mathbf{n}-\mathbf{k}} G_{\mathbf{k},\mathbf{m}}^{-1}, \ \mathbf{n} \in \mathcal{I}_g, \ \mathbf{m} \in \mathcal{I}_b.$$

4. Truncated time-dependent problem. Performing the Laplace transform on (2.10) and recalling (2.7), we have

(4.1) 
$$s^{2}\hat{q}_{\mathbf{n}} + \sum_{|\mathbf{m}| \le L} c_{\mathbf{m}}\hat{q}_{\mathbf{n}-\mathbf{m}} = 0, |\mathbf{n}| > M,$$

$$\lim_{|\mathbf{n}| \to \infty} \hat{q}_{\mathbf{n}} = 0.$$

This problem is in the form of problem (3.1)–(3.2) with  $z = s^2$ . By the expression (3.4), for all  $s^2 \notin \sigma(-\mathcal{T})$ , it holds that

(4.3) 
$$\hat{q}_{\mathbf{n}}(s) = \sum_{\mathbf{m} \in \mathcal{I}_b} \mathcal{K}_{\mathbf{n},\mathbf{m}} \left(s^2\right) \hat{q}_{\mathbf{m}}(s), \ \mathbf{n} \in \mathcal{I}_g.$$

Let  $\Omega$  be a simply connected domain with boundary  $\Gamma$  in the s-complex plane, such that  $s^2 \notin \sigma(-\mathcal{T})$  for all  $s \in \mathbb{C} \setminus \overline{\Omega}$ . By the Cauchy integral formula, it holds that

$$\mathcal{K}_{\mathbf{n},\mathbf{m}}\left(s^{2}\right) = \frac{1}{2\pi i} \int_{\Gamma} \frac{\mathcal{K}_{\mathbf{n},\mathbf{m}}(\xi^{2})}{s - \xi} d\xi \ \forall s \in \mathbb{C} \backslash \bar{\Omega}.$$

Substituting the above into (4.3) and performing the inverse Laplace transform, we obtain

(4.4) 
$$q_{\mathbf{n}} = \frac{1}{2\pi i} \sum_{\mathbf{m} \in \mathcal{I}_b} \int_{\Gamma} \mathcal{K}_{\mathbf{n}, \mathbf{m}} \left( \xi^2 \right) \left[ e^{\xi t} * q_{\mathbf{m}} \right] d\xi, \ \mathbf{n} \in \mathcal{I}_g.$$

Taking the above as a boundary condition, we then derive a truncated problem

$$(4.5) \quad \partial_t^2 q_{\mathbf{n}} + \sum_{|\mathbf{m} - \mathbf{n}| \le L} a_{\mathbf{n}, \mathbf{m}} q_{\mathbf{m}} = f(x_{\mathbf{n}}, t), \ |\mathbf{n}| \le M, \ 0 < t \le T,$$

(4.6) 
$$q_{\mathbf{n}} = \frac{1}{2\pi i} \sum_{\mathbf{m} \in \mathcal{I}_b} \int_{\Gamma} \mathcal{K}_{\mathbf{n}, \mathbf{m}} \left( \xi^2 \right) \left[ e^{\xi t} * q_{\mathbf{m}} \right] d\xi, \ \mathbf{n} \in \mathcal{I}_g,$$

(4.7) 
$$\partial_t^k q_{\mathbf{n}}(0) = \psi_k(\mathbf{x_n}), \ |\mathbf{n}| \le M, \ k \in \{0, 1\}.$$

Introducing

$$g_{\mathbf{m},\xi} = e^{\xi t} * q_{\mathbf{m}}, \ \mathbf{m} \in \mathcal{I}_b, \ \xi \in \Gamma,$$

we can rewrite the truncated problem (4.5)–(4.7) in the following form:

(4.8) 
$$\partial_t^2 q_{\mathbf{n}} + \sum_{|\mathbf{m}| \le L} a_{\mathbf{n}, \mathbf{m}} q_{\mathbf{m}} = f(x_{\mathbf{n}}, t), \ |\mathbf{n}| \le M, \ 0 < t \le T,$$

(4.9) 
$$\partial_t g_{\mathbf{m},\xi} = \xi g_{\mathbf{m},\xi} + q_{\mathbf{m}}, \ g_{\mathbf{m},\xi}(0) = 0, \ \mathbf{m} \in \mathcal{I}_b, \ \xi \in \Gamma,$$

(4.10) 
$$q_{\mathbf{n}} = \frac{1}{2\pi i} \sum_{\mathbf{m} \in \mathcal{I}} \int_{\Gamma} \mathcal{K}_{\mathbf{n}, \mathbf{m}} \left(\xi^{2}\right) g_{\mathbf{m}, \xi} d\xi, \ \mathbf{n} \in \mathcal{I}_{g},$$

(4.11) 
$$\partial_t^k q_{\mathbf{n}}(0) = \psi_k(\mathbf{x}_{\mathbf{n}}), |\mathbf{n}| \le M, k \in \{0, 1\}.$$

After employing an appropriate quadrature scheme for the contour integral, we get a discrete ODE system that can be solved numerically using a suitable ODE solver like the Verlet-type integrators to ensure both stability and accuracy.

5. Numerical scheme. Concerning the implementation of the discretization scheme, there are many issues worthy of further consideration. In particular, the contour  $\Gamma$  involved in (4.10) should be carefully chosen and the quadrature scheme must be carefully designed. Since these issues are problem dependent, we use some examples to explain the main strategy.

First, a Gaussian kernel function is used in [32] as

$$\gamma_0(\mathbf{x}) = 10 \exp\left(-20|\mathbf{x}|^2\right), \ \gamma(\mathbf{x}, \mathbf{y}) = \gamma_0(\mathbf{x} - \mathbf{y}), \ \mathbf{x}, \mathbf{y} \in \mathbb{R}^2.$$

It is easy to check that the dispersive relation for the nonlocal wave problem is

$$\omega^2 = \int_{\mathbb{R}^2} [1 - \exp(i\mathbf{k} \cdot \mathbf{x})] \gamma_0(\mathbf{x}) d\mathbf{x} = \frac{\pi}{2} \left[ 1 - \exp\left(-\frac{|\mathbf{k}|^2}{80}\right) \right],$$

where  $\mathbf{k}$  denotes the wavenumber vector. The above dispersive relation reveals that unlike the local wave equation, the nonlocal wave equation is actually dispersive.

The numerical experiments are performed for (2.2) with further simplifications. In the case that the kernel  $\gamma$  is smooth and the horizon  $\delta$  is of order one, we can use quadratures such as the following composite trapezoidal quadrature

(5.1) 
$$\int g(\mathbf{x})d\mathbf{x} \sim h^2 \sum_{\mathbf{m} \in \mathbb{Z}^2} g(\mathbf{x_m}).$$

In this situation, we have

$$a_{\mathbf{n},\mathbf{m}} = \left\{ \begin{array}{ll} h^2 \sum_{\mathbf{k} \neq \mathbf{0}} \gamma_0(\mathbf{x}_{\mathbf{k}}), & \mathbf{n} = \mathbf{m}, \\ -h^2 \gamma_0(\mathbf{x}_{\mathbf{n} - \mathbf{m}}), & \mathbf{n} \neq \mathbf{m}. \end{array} \right.$$

For smooth kernels, this simplification maintains the same order of numerical accuracy.

Since the matrix  $(a_{\mathbf{n},\mathbf{m}})$  is diagonally dominant, we know that the spectrum  $\sigma(\mathcal{T})$  lies on the right half of the real axis. Besides, it is straightforward to check that for suitably small spatial step size h, the spectrum  $\sigma(\mathcal{T})$  has a uniform upper bound

$$2\int_{\mathbb{R}^2} \gamma_0(\mathbf{x}) d\mathbf{x} = \pi.$$

Moreover, considering that the Gaussian function decays extremely fast, we again simplify the computation by truncating the support of the kernel function  $\gamma_0$  and set the horizon range as  $\delta = 1$ .

The boundedness of  $\sigma(-\mathcal{T})$  allows us to choose a closed contour integral for (4.10). In the following simulations, we take a rectangular integral path with  $\Re(\xi) \in [-0.3, 0.3]$  and  $\Im(\xi) \in [-4, 4]$  (see Figure 2), and use the Gauss–Legendre quadrature for each edge of the rectangular contour. The resulting quadrature approximation of (4.10) is denoted by

(5.2) 
$$q_{\mathbf{n}} = \sum_{\xi \in \mathcal{P}} w_{\xi} \sum_{\mathbf{m} \in \mathcal{I}_b} \mathcal{K}_{\mathbf{n}, \mathbf{m}} g_{\mathbf{m}, \xi}, \ \mathbf{n} \in \mathcal{I}_g,$$

where  $\mathcal{P}$  stands for the set of poles and  $w_{\mathcal{E}}$  is the associated quadrature weight.

We divide the computational time interval [0,T] over a set of discrete time steps  $\Omega_t := \{t_n, n = 0, 1, \dots, J\}$  with  $t_0 = 0, t_J = T$ , and the temporal size  $\tau = T/J$ . The

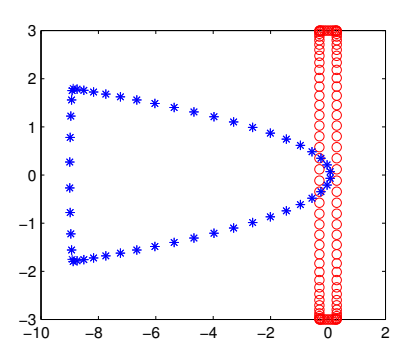


Fig. 2. Integrating contour. The red dots form the integrating contour. The blue dots stand for the square of the Laplace variable, i.e.,  $z=s^2$ . The Gauss-Legendre quadrature is used for each edge of the rectangular contour.

approximation of  $q(\mathbf{x_n}, t_j)$  is simply denoted by  $q_{\mathbf{n}}^j$ , and the value of  $f(\mathbf{x_n}, t_j)$  by  $f_{\mathbf{n}}^j$ . The Verlet algorithm [29] is adopted to integrate (4.8) in time:

(5.3) 
$$q_{\mathbf{n}}^{j+1} = q_{\mathbf{n}}^{j} + \tau \partial_{t} q_{\mathbf{n}}^{j} - \frac{\tau^{2}}{2} \left( \sum_{|\mathbf{m}| \leq L} a_{\mathbf{n},\mathbf{m}} q_{\mathbf{m}}^{j} - f_{\mathbf{n}}^{j} \right), |\mathbf{n}| \leq M,$$

$$(5.4) \quad \partial_t q_{\mathbf{n}}^{j+1} = \partial_t q_{\mathbf{n}}^j - \frac{\tau}{2} \left( \sum_{|\mathbf{m}| \leq L} a_{\mathbf{n},\mathbf{m}} \left( q_{\mathbf{m}}^j + q_{\mathbf{m}}^{j+1} \right) - f_{\mathbf{n}}^j - f_{\mathbf{n}}^{j+1} \right), |\mathbf{n}| \leq M.$$

The initial values are set as

$$q_{\mathbf{n}}^0 = \psi_0(\mathbf{x}_{\mathbf{n}}), \ \partial_t q_{\mathbf{n}}^0 = \psi_1(\mathbf{x}_{\mathbf{n}}), \ |\mathbf{n}| \le M.$$

The value of  $q_{\mathbf{n}}^{j}$  with  $\mathbf{n} \in \mathcal{I}_{g}$  involved in (5.3), i.e.,  $M < |\mathbf{n}| \leq M + L$ , is determined by the quadrature approximation (5.2) via

(5.5) 
$$q_{\mathbf{n}}^{j} = \sum_{\xi \in \mathcal{P}} w_{\xi} \sum_{\mathbf{m} \in \mathcal{I}_{b}} \mathcal{K}_{\mathbf{n}, \mathbf{m}} g_{\mathbf{m}, \xi}^{j}, \ \mathbf{n} \in \mathcal{I}_{g}.$$

To derive the approximation of  $g_{\mathbf{m},\xi}$  at time  $t_{j+1}$ , we discretize (4.9) by using the Crank–Nicolson scheme

(5.6) 
$$\frac{g_{\mathbf{m},\xi}^{j+1} - g_{\mathbf{m},\xi}^{j}}{\tau} = \xi \frac{g_{\mathbf{m},\xi}^{j+1} + g_{\mathbf{m},\xi}^{j}}{2} + \frac{q_{\mathbf{m}}^{j+1} + q_{\mathbf{m}}^{j}}{2}, \ \mathbf{m} \in \mathcal{I}_{b}, \ \xi \in \mathcal{P}.$$

The initial value is set as  $g_{\mathbf{m},\xi}^0 = 0$ .

Instead of computing the DtD mappings  $\mathcal{K}_{\mathbf{n},\mathbf{m}}$  explicitly in (5.5), we evaluate their actions by solving a sequence of linear algebraic systems; see the definition (3.4). This treatment becomes indispensable when the involved number of degrees of freedom is large. In the numerical simulations reported in the next section, we use GMRES to solve the resulting discrete algebraic equations.

6. Numerical examples. To illustrate the effectiveness of our DtD-type boundary conditions, we present four numerical examples. In the first three examples, we plot the numerical solutions and history errors at different times, and also investigate the convergence of the numerical scheme. In the last example, we present the numerical simulations at different times by setting the initial value discontinuous. In the

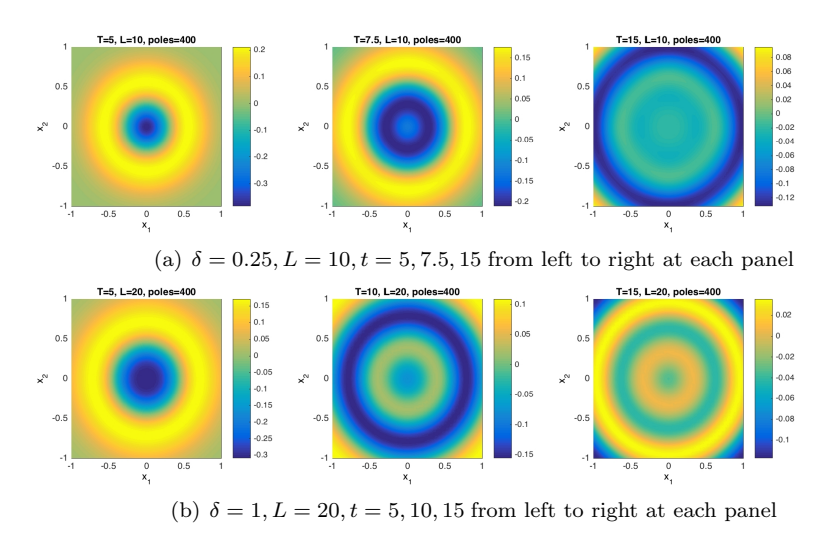


Fig. 3. (Example 1): Numerical solutions at different times.

simulations, the computational domain is taken as  $[-1,1] \times [-1,1]$ , and the initial values are selected to be compactly supported in this domain or they are negligible outside of this domain. We now define the  $L^2$ -error and convergence order by

$$L^{2}\operatorname{-error}(h) = \sqrt{\sum_{|\mathbf{n}| \le M + L} (u_{\mathbf{n}}^{\operatorname{nu}} - u_{\mathbf{n}}^{\operatorname{ex}}, u_{\mathbf{n}}^{\operatorname{nu}} - u_{\mathbf{n}}^{\operatorname{ex}})_{\mathfrak{H}}},$$
$$r_{s} = \log\left(\frac{L^{2}\operatorname{-error}(h_{1})}{L^{2}\operatorname{-error}(h_{2})}\right) / \log\left(\frac{h_{2}}{h_{1}}\right),$$

where  $u_{\mathbf{n}}^{\text{nu}}$  represents the solution of (4.8)–(4.11), and  $u_{\mathbf{n}}^{\text{ex}}$  represents the "exact" solution. The exact solution is obtained by using the spectral method in a large computational domain with sufficiently fine mesh sizes. As we will see in Examples 1–3, our scheme is the second-order accurracy by fixing  $\Delta t = h/2$  and refining h with various initial values.

Example 1. In this example, we take a circularly shaped scalar wave. The initial velocity  $\psi_1(x)$  is set to be zero while the initial position is taken as

$$\psi_0(x) = \exp(-10(x^2 + y^2)).$$

Figure 3 shows the numerical solutions at different times for  $\delta = 0.25, 1$ , respectively. As one can see in Figure 3, the ABCs allow the wave to pass through the artificial layers and there are no obvious reflected waves.

To investigate the accuracy of ABCs, the  $L^2$ -errors in each time step are plotted in Figure 4. As one can see in Figure 4, the  $L^2$ -error becomes smaller and smaller while refining the mesh size h. The  $L^2$ -errors and convergence orders at time T=15 are shown in Table 1 by increasing L, i.e., reducing  $h=\delta/L$ , for given  $\delta=1$  and taking  $\tau=h/2$ . Table 1 implies that solutions of numerical schemes (4.8)–(4.11) converge to exact solutions with second-order accuracy when refining the mesh. We point out that almost the same convergence order can be observed at different times and for different  $\delta$ 's. For brevity, we will not present the results in the context here and below.

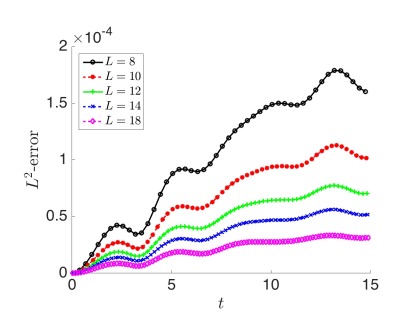


Fig. 4. (Example 1): The evolution of  $L^2$ -errors at each time step.

Table 1 (Example 1)  $L^2$ -errors and convergence orders by increasing M for given  $\delta = 1$  at time T = 10.

$\overline{M}$	8	10	12	14	18
$L^2$ -errors	$1.61 \times 10^{-4}$	$1.02 \times 10^{-4}$	$7.10 \times 10^{-5}$	$5.21 \times 10^{-5}$	$3.15 \times 10^{-5}$
Order	_	2.02	2.01	2.01	2.00

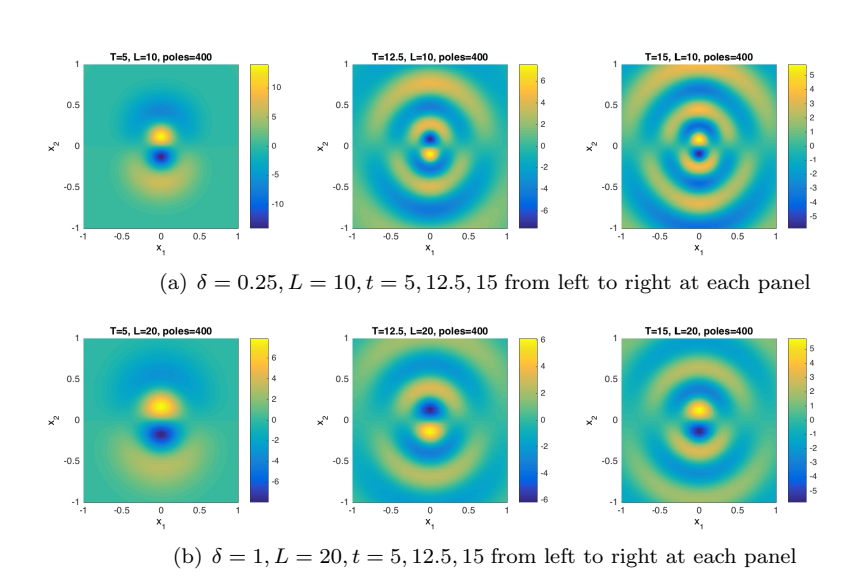


Fig. 5. (Example 2): The solutions at different times.

Example 2. We now consider a wave in double-layer media as shown in [15]. The initial value is set as  $\psi_0(x) = 0$  and the initial velocity is set as

$$\psi_1(x) = 25 \exp\left(-50\left(x^2 + (y+0.1)^2\right)\right) - 25 \exp\left(-50\left(x^2 + (y-0.1)^2\right)\right).$$

Again, Figure 5 shows numerical solutions at different times for  $\delta=0.25,1$ , respectively. No obvious reflection is observed. The  $L^2$ -errors in each time step are plotted in Figure 6, in which the  $L^2$ -error becomes smaller and smaller while increasing the mesh grid points. Furthermore, the  $L^2$ -errors and the second-order convergence at time T=15 are shown in Table 2 by reducing  $h=\delta/M$  for given  $\delta=1$  and taking  $\tau=h/2$ .

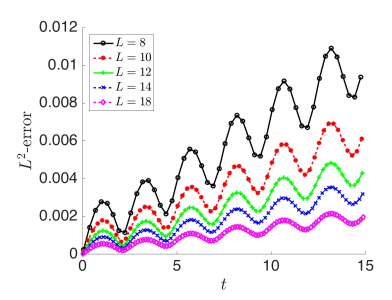


Fig. 6. (Example 2): The evolution of  $L^2$ -errors at each time step.

Table 2 (Example 2)  $L^2$ -errors and convergence orders by increasing M for given  $\delta = 1$  at time T = 15.

$\overline{M}$	8	10	12	14	18
$L^2$ -errors	$1.06 \times 10^{-2}$	$6.74 \times 10^{-3}$	$4.67 \times 10^{-3}$	$3.42 \times 10^{-3}$	$2.07 \times 10^{-3}$
Order	_	2.02	2.01	2.01	2.00

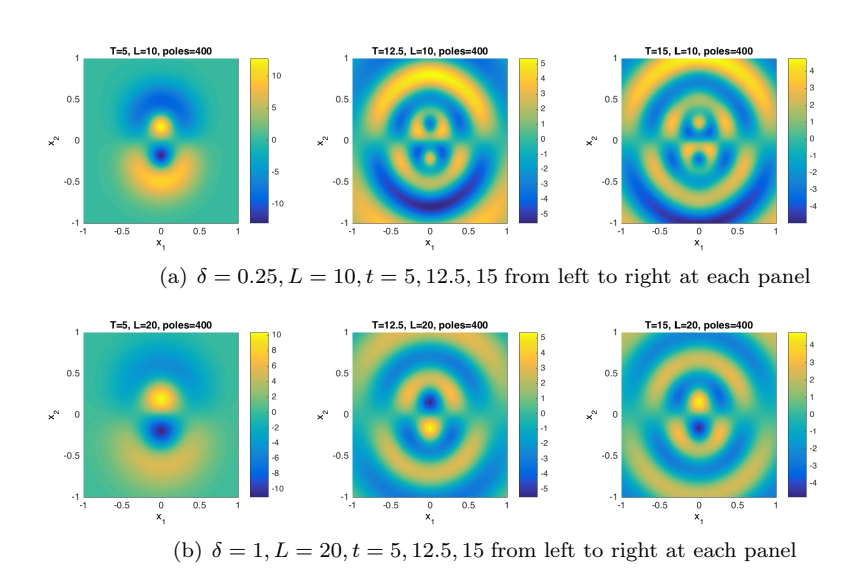


Fig. 7. (Example 3): Numerical solutions at different times.

Example 3. We consider a wave with both nonvanishing initial values, namely,

$$\psi_0(x) = \exp\left(-10\left((x+0.2)^2 + (y+0.2)^2\right)\right) + \exp\left(-10\left((x-0.2)^2 + (y-0.2)^2\right)\right),$$
  
$$\psi_1(x) = 25\exp\left(-50\left(x^2 + (y+0.2)^2\right)\right) - 25\exp\left(-50\left(x^2 + (y-0.2)^2\right)\right).$$

Again, Figure 7 shows numerical solutions at different times for  $\delta=0.25,1$ , respectively. No obvious reflection is observed. The  $L^2$ -errors in each time step are plotted in Figure 8, in which, the  $L^2$ -error becomes smaller and smaller while increasing the mesh grid points. Furthermore, the  $L^2$ -errors and the second-order convergence at time T=15 are shown in Table 3 by refining  $h=\delta/L$  for given  $\delta=1$  and taking  $\tau=h/2$ .

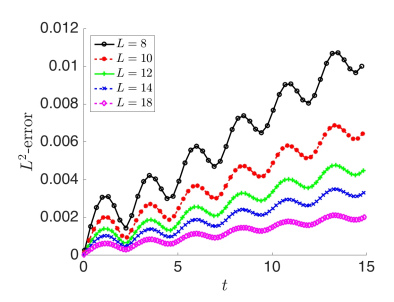


Fig. 8. (Example 3): The evolution of  $L^2$ -errors at each time step.

Table 3 (Example 3)  $L^2$ -errors and convergence orders by increasing M for given  $\delta = 1$  at time T = 15.

$\overline{M}$	8	10	12	14	18
$L^2$ -errors	$1.06 \times 10^{-2}$	$6.74 \times 10^{-3}$	$4.67 \times 10^{-3}$	$3.42 \times 10^{-3}$	$2.07 \times 10^{-3}$
Order		2.02	2.02	2.03	2.01

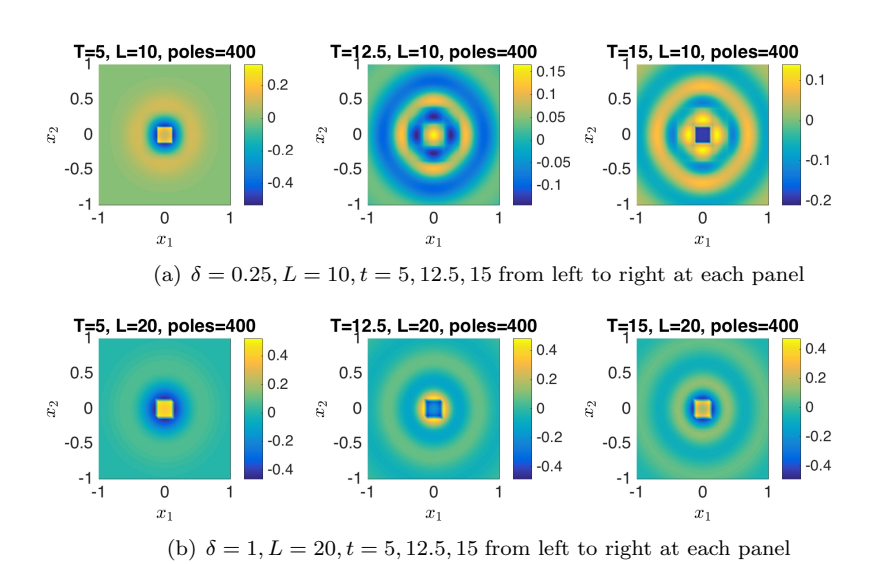


Fig. 9. (Example 4): The numerical solutions at different times.

Example 4. We now consider the initial velocity  $\psi_1(x) = 0$  and the initial positions are discontinuous as

$$\psi_0(x) = \begin{cases} 1, & |x_1| \le \frac{1}{4}, |x_2| \le \frac{1}{4}, \\ 0, & \text{otherwise.} \end{cases}$$

Since the initial wave profile is discontinuous, it is not feasible to obtain the reference solution of the nonlocal model analytically. In this example, we present numerical solutions at different times for  $\delta=0.25,1$  in Figure 9, respectively. Again, one can see that the wave approaches artificial boundaries and there is no obvious reflection that would affect the solution in the interior computational domain taken here.

7. Conclusion. The numerical solution of initial-value problems for a nonlocal wave equation in unbounded spatial domains is studied in this paper. The effectiveness and accuracy of the corresponding numerical scheme depend on the design of suitable ABCs. This paper presents a new method to derive such ABCs for nonlocal wave equations in two dimensions. We first derive a semidiscrete nonlocal wave equation after employing AC quadrature scheme developed in [24, 8] for the spatial nonlocal interaction. By resorting to the idea of a first-kind integral equation method, we then obtain a generalized DtD mapping from the artificial layer to the ghost layer in the Laplace domain. After discretizing the contour integrals used in the inverse Laplace transform, we end up with an approximate DtD mapping in the time domain. Taking this DtD mapping as an ABC, we get a truncated semidiscrete nonlocal wave problem which only involves a finite number of degrees of freedom. A Verlet-type ODE solver is used for the time integration. Some numerical examples are performed to illustrate the efficiency and accuracy of the proposed numerical approach.

There are a number of interesting issues to be studied further. First, the theoretical convergence of the algorithm can be pursued. Second, more quantitative investigations on wave propagations in the nonlocal wave models can be carried out. Comparisons with the properties of the local wave equation are also interesting to make [9]. Another important issue is to speed up the evaluation of convolution in our ABCs given its high computational cost. We may consider possible speedups in two aspects: (a) the convolution of the DtD mapping may be constructed as a matrix multiplication, where one of the inputs is converted into a Toeplitz matrix, which allows the application of FFTs; (b) in light of the structure of the DtD map, the idea of fast multipole methods may also be used. In addition, efficient implementations in three space dimensions are also important for practical applications.

## REFERENCES

- [1] O. Weckner and R. Abeyaratne, The effect of long-range forces on the dynamics of a bar, J. Mech. Phys. Solids, 53 (2005), pp. 705–728.
- [2] B. Alpert, L. Greengard, and T. Hagstrom, Rapid evaluation of nonreflecting boundary kernels for time-domain wave propagation, SIAM J. Numer. Anal., 37 (2000), pp. 1138– 1164.
- [3] A. Arnold, M. Ehrhardt, and I. Sofronov, Approximation, stability and fast calculation of nonlocal boundary conditions for the Schrödinger equation, Commun. Math. Sci., 1 (2003), pp. 501–556.
- [4] F. Bobaru and M. Duangpanya, The peridynamic formulation for transient heat conduction, Int. J. Heat Mass Transf., 53 (2010), pp. 4047–4059.
- [5] X. CHEN AND M. GUNZBURGER, Continuous and discontinuous finite element methods for a peridynamics model of mechanics, Comput. Methods Appl. Mech. Engrg., 200 (2011), pp. 1237–1250.
- [6] Q. Du, M. Gunzburger, R.B. Lehoucq, and K. Zhou, Analysis and approximation of nonlocal diffusion problems with volume constraints, SIAM Rev., 54 (2012), pp. 667–696.
- [7] Q. Du, M. Gunzburger, R.B. Lehoucq, and K. Zhou, A nonlocal vector calculus, nonlocal volume-constrained problems, and nonlocal balance laws, Math. Models Method Appl. Sci., 23 (2013), pp. 493–540.
- [8] Q. Du, Y. Tao, X. Tian, and J. Yang, Asymptotically compatible discretization of multidimensional nonlocal diffusion models and nonlocal gradient recovery, IMA J. Numer. Amal., to appear.
- [9] Q. Du, J. Zhang, and C. Zheng, Nonlocal wave propagation in unbounded multi-scale mediums, Commun. Comput. Phys., to appear.
- [10] E. EMMRICH AND O. WECKNER, Analysis and numerical approximation of an integrodifferential equation modeling non-local effects in linear elasticity, Math. Mech. Solids, 12 (2007), pp. 363–384.

- [11] D. GIVOLI, High-order local non-reflecting boundary conditions: A review, Wave Motion 39 (2004), pp. 319–326.
- [12] I. S. GRADSHTEYN AND I. M. RYZHIK, Tables of Integrals, Series, and Products, 6th ed., Academic Press, San Diego, CA, 2000, p. 1090.
- [13] M. J. GROTE AND J. B. KELLER, Exact nonreflecting boundary conditions for the time dependent wave equation, SIAM J. Appl. Math., 55 (1995), pp. 280–297.
- [14] T. HAGSTROM, New results on absorbing layers and radiation boundary conditions, in Topics in Computational Wave Propagation, M. Ainsworth et al., eds., Springer, New York, 2003, pp. 1–42.
- [15] T. HAGSTROM, A. MAR-OR, AND D. GIVOLI, High-order local absorbing conditions for the wave equation: Extensions and improvements, J. Comput. Phys., 227 (2008), pp. 3322–3357.
- [16] H. HAN AND Z. HUANG, A class of artificial boundary conditions for heat equation in unbounded domains, Comput. Math. Appl., 43 (2002), pp. 889–900.
- [17] H. HAN AND X. WU, Artificial Boundary Method, Springer, Heidelberg, 2013.
- [18] H. D. HAN AND C. ZHENG, Exact nonreflecting boundary conditions for an acoustic problem in three dimensions, J. Comput. Math., 21 (2003), pp. 15–24.
- [19] S. G. Krantz, Handbook of Complex Variables, Birkhäuser, Boston, MA, 1999.
- [20] R. W. MACEK AND S. SILLING, Peridynamics via finite element analysis, Finite Elem. Anal. Des., 43 (2007), pp. 1169–1178.
- [21] G. Pang, Y. Yang, and S. Tang, Exact boundary condition for semi-discretized Schrödinger equation and heat equation in a rectangular domain, J. Sci. Comput., 72 (2017), pp. 1–13.
- [22] S. SILLING, Reformulation of elasticity theory for discontinuities and long-range forces, J. Mech. Phys. Solids, 48 (2000), pp. 175–209.
- [23] Z. H. Teng, Exact boundary condition for time-dependent wave equation based on boundary integral, J. Comput. Phys., 190 (2003), pp. 398–418.
- [24] X. Tian and Q. Du, Analysis and comparison of different approximations to nonlocal diffusion and linear peridynamic equations, SIAM J. Numer. Anal., 51 (2013), pp. 3458–3482.
- [25] X. Tian and Q. Du, Asymptotically compatible schemes and applications to robust discretization of nonlocal models, SIAM J. Numer. Anal., 52 (2014), pp. 1641–1665.
- [26] H. Tian, L. Ju, and Q. Du, A conservative nonlocal convection-diffusion model and asymptotically compatible finite difference discretization, Comput. Methods Appl. Mech. Engrg., 320 (2017), pp. 46–67.
- [27] L. Ting and M. J. Miksis, Exact boundary conditions for scattering problems, J. Acoust. Soc. Amer., 80 (1986), 1825-1827.
- [28] S. V. TSYNKOV, Numerical solution of problems on unbounded domains: A review, Appl. Numer. Math., 27 (1998), pp. 465-532.
- [29] L. Verlet, Computer experiments on classical fluids. I. Thermodynamical properties of Lennard-Jones molecules, Phys. Rev. (2), 159 (1967), pp. 98–103.
- [30] V. VILLAMIZAR, S. ACOSTA, AND B. DASTRUP, High order local absorbing boundary conditions for acoustic waves in terms of farfield expansions, J. Comput. Phys., 333 (2017), pp. 331– 351.
- [31] X. WANG AND S. TANG, Matching boundary conditions for lattice dynamics, Internat. J. Numer Methods Engrg., 93 (2013), pp. 1255–1285.
- [32] R. A. WILDMAN AND G. A. GAZONAS, A perfectly matched layer for peridynamics in two dimensions, J. Mech. Mater. Struct., 7 (2012), pp. 765–781.
- [33] X. Wu and J. Zhang, High-order local absorbing boundary conditions for heat equation in unbounded domains, J. Comput. Math., 29 (2011), pp. 74–90.
- [34] W. ZHANG, J. YANG, J. ZHANG, AND Q. Du, Absorbing boundary conditions for nonlocal heat equations on unbounded domain, Commun. Comput. Phys., 21 (2017), pp. 16–39.
- [35] C. ZHENG, J. HU, Q. DU, AND J. ZHANG, Numerical Solution of the Nonlocal Diffusion Equation on the Real Line, SIAM J. Sci. Comput., 39 (2017), pp. A1951–A1968.
- [36] K. Zhou and Q. Du, Mathematical and numerical analysis of linear peridynamic models with nonlocal boundary conditions, SIAM J. Numer. Anal., 48 (2010), pp. 1759–1780.